Journal of Alloys and Compounds 504S (2010) S234–S238

Contents lists available at ScienceDirect

Journal of Alloys and Compounds

journal homepage: www.elsevier.com/locate/jallcom

TEM study of the cooling rate dependent crystallization behavior of $(Zr_{65}Al_{10}Ni_{10}Cu_{15})_{98}Nb_2$ metallic glass

Yingmin Wang[a,*], Chan Hung Shek[b], Qing Wang[a], Jianbing Qiang[a], Chuang Dong[a]

[a] School of Materials Science and Engineering, Dalian University of Technology, No. 2 Lingggong Road, Ganjingzi District, Dalian, Liaoning 116024, China
[b] Department of Physics and Materials Science, City University of Hong Kong, Hong Kong SAR, China

ARTICLE INFO

Article history:
Received 20 October 2009
Received in revised form 28 February 2010
Accepted 18 March 2010
Available online 25 March 2010

Keywords:
Metallic glasses
Quasicrystals
Crystallization
Transmission electron microscopy

ABSTRACT

The crystallization of $(Zr_{65}Al_{10}Ni_{10}Cu_{15})_{98}Nb_2$ metallic glasses has been studied using transmission electron microscopy (TEM), X-ray diffraction (XRD) and differential scanning calorimetry (DSC). The ribbon glass and bulk metallic glass (BMG) of this alloy exhibit different crystallization behaviors. For ribbon glass in the first stage crystallization, icosahedral quasicrystal (I-phase) precipitated together with the η-Zr_2Ni (a = 1.226 nm) phase. The BMG alloy transforms into the I-phase and two coherently coexisted phases, namely, the Al_2Zr_3 phase and an unknown primitive cubic phase (a = 0.76 nm) in this stage. The experimental evidence indicates that the liquid cooling rate for sample preparation has a significant effect on its crystallization behavior of this alloy glass.

1. Introduction

Bulk metallic glasses (BMGs) have been discovered in a wide variety of alloy systems in the past two decades [1–3]. These alloys are metastable, but are sufficiently stable against crystallization to exhibit wide undercooled liquid spans, $\Delta T_x = T_x - T_g$, where T_g is the calorimetric glass transition temperature and T_x is the temperature at which the undercooled liquid state is terminated by a crystallization event. Their atomic scale structures are poorly known. In some Zr-based BMGs, metastable icosahedral quasicrystals (I-phases) can form in their devitrification processes. Köster et al. first reported the formation of I-phase in a $Zr_{69.5}Al_{7.5}Ni_{11}Cu_{12}$ BMG annealed within the undercooled liquid region [4]. Subsequently, ample experimental evidence has revealed that I-phase formation in Zr–Al–Ni–Cu alloys is favored by the addition of oxygen [5], noble metals such as Ag, Pd, Pt and Au [6–9], and the transition metals Nb, Ta, V, and Ti [10–12]. In view of Frank's hypothesis that icosahedral atomic clustering in these undercooled liquids is energetically favored [13], glass-to-I-phase transformation in these alloys sheds some light on understanding the local structures of Zr-based BMGs and their formations as well.

Since these I-phases are metastable, liquid undercooling is a necessary precondition for their formations during liquid cooling and, hence I-phase would appear to compete with BMG formation. Though the onset formation temperature of I-phase and the location of T_g are significant parameters for BMG formation, they are hardly detectable during the liquid cooling down path. Mostly, I-phase formation is observed when annealing a metallic glass within the undercooled liquid region in a heating up process. The thermal histories of metallic glasses would affect the crystallization behavior. For instance, Xing et al. reported that the precipitation of I-phase from a $Zr_{57}Cu_{20}Al_{10}Ni_8Ti_5$ metallic glass is cooling rate dependent [14]. In particular, the slowly cooled $Zr_{57}Cu_{20}Al_{10}Ni_8Ti_5$ BMG transforms into an I-phase in the first stage crystallization, which follows a polymorphic transformation mechanism; the rapidly quenched ribbon glass of this alloy, however, transforms into a mixture of I-phase, Zr_2Cu and Zr_2Ni intermetallic compounds in this stage. In the present work, we report the different phase transformation behaviors of $(Zr_{65}Al_{10}Ni_{10}Cu_{15})_{98}Nb_2$ metallic glasses of ribbon and bulk forms.

2. Experimental

The purities of the staring materials are 99.9 wt.% for Zr, 99.999 wt.% for Al and 99.99 wt.% for Cu, Ni and Nb. $(Zr_{65}Al_{10}Ni_{10}Cu_{15})_{98}Nb_2$ alloy ingots were prepared by arc melting the mixture of these pure metals under a vacuum level of about 5×10^{-3} Pa. Zr–Nb intermediate alloy with an appropriate quantity of Nb was first prepared. The intermediate alloy and proper quantities of Zr, Al, Ni and Cu were then repeatedly melted to make homogenous alloy ingots of the desired composition. The total weight losses of these samples after arc melting were measured to be less than about 0.05%. Using the ingots, ribbons of averagely 30 μm in thickness and 1.5 mm in width were prepared by means of melt-spinning, and 3 mm diameter alloy rods were made using a copper mould suction casting equipment. X-ray (Cu Kα irradiation, λ = 0.15406 nm) diffraction (XRD) for phase identification was performed on the as-cast and annealed samples via θ–2θ scans. Specimens for transmission electron microscopy (TEM) were prepared by standard twin-jet electrolytic thinning with a $HClO_4$–CH_3OH–C_2H_5OH electrolyte (volume ratio 1:1:9). Thermal

* Corresponding author. Tel.: +86 411 84709336; fax: +86 411 84708389.
E-mail address: apwangym@dlut.edu.cn (Y. Wang).

0925-8388/$ – see front matter © 2010 Elsevier B.V. All rights reserved.
doi:10.1016/j.jallcom.2010.03.162

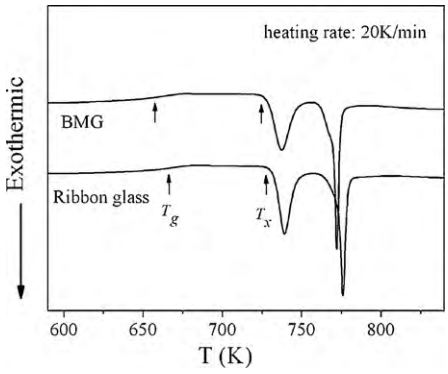

Fig. 1. Constant heating rate DSC traces of the $(Zr_{65}Al_{10}Ni_{10}Cu_{15})_{98}Nb_2$ ribbons and 3 mm diameter BMG rods. The glass transition and the onset crystallization temperatures are indicated by arrows.

analysis was carried out on a Perkin-Elmer 7 differential scanning calorimeter (DSC) at a constant heating rate of 20 K/min. Microstructure observation was performed on a Tecnai $20G^2$ transmission electron microscope (TEM) attached with an Oxford Energy Dispersive X-ray spectroscopy (EDX) system.

3. Results and discussion

X-ray diffraction and TEM observations revealed that the $(Zr_{65}Al_{10}Ni_{10}Cu_{15})_{98}Nb_2$ ribbon samples and the 3 mm diameter as-cast rods were amorphous in nature. Their DSC traces obtained at a constant heating rate of 20 K/min (Fig. 1) show that upon heating, both the ribbon glass and the BMG samples of this alloy undergo a distinct glass transition before entering into the undercooled liquid state, indicating their glass natures. The ribbon glass exhibits a glass transition at T_g = 659 K, which is higher than that (T_g = 654 K) of the BMG sample. Their undercooled liquid states were terminated by two successive crystallization events with onset temperatures of 733 K for ribbon and 729 K for BMG. Wide undercooled liquid regions exceeding 70 K are observed in these metallic glasses regardless of their different preparation conditions.

Isothermal annealing experiments were conducted within their undercooled liquid regions to explore structure transformation. The XRD patterns in Fig. 2(a) show that the 673 K-30 min annealed sample was apparently amorphous. I-phase precipitates in the sample after 5 min annealing at 703 K. At even higher temperatures within the undercooled liquid region, for instance 723 K, the glass-to-I-phase transformation proceeds more rapidly. After prolonged annealing, new diffraction peaks, which cannot be indexed to the I-phase, appear, indicating the precipitation of crystalline phases. These new XRD peaks can be tentatively indexed to a η-Zr_2Ni type phase [15]. The non-isothermal annealing process for the ribbon glass was done in the DSC chamber. The ribbon sample was heated at a constant rate of 20 K/min to the end of the first exothermic reaction (768 K), and then rapidly cooled down to room temperature at a rate of 200 K/min. The XRD pattern taken from the non-isothermal

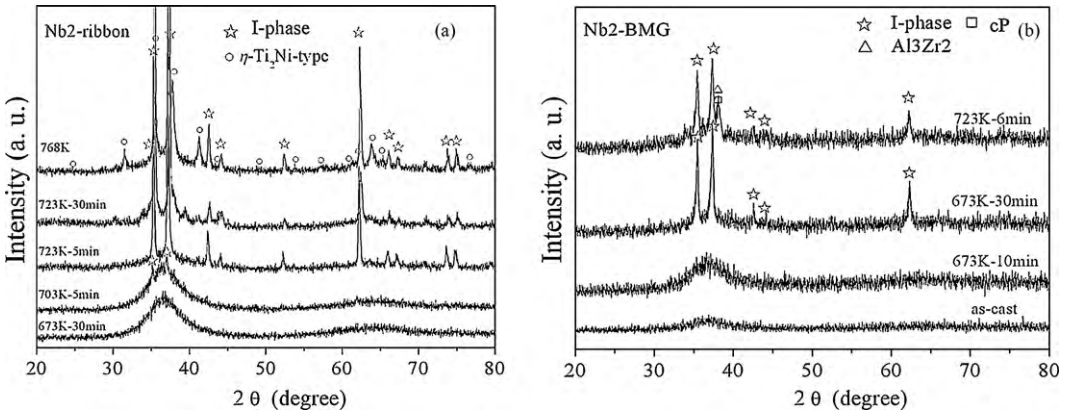

Fig. 2. (a) XRD patterns of the ribbon glasses annealed at 673 K, 703 K, 723 K, and 723 K, respectively. The upmost pattern was taken from the sample obtained by heating up to 768 K at 20 K/min and by subsequent cooling down to room temperature at 200 K/min. (b) XRD patterns of the 3 mm diameter BMGs annealed at 673 K, 703 K and 723 K for different annealing time, respectively.

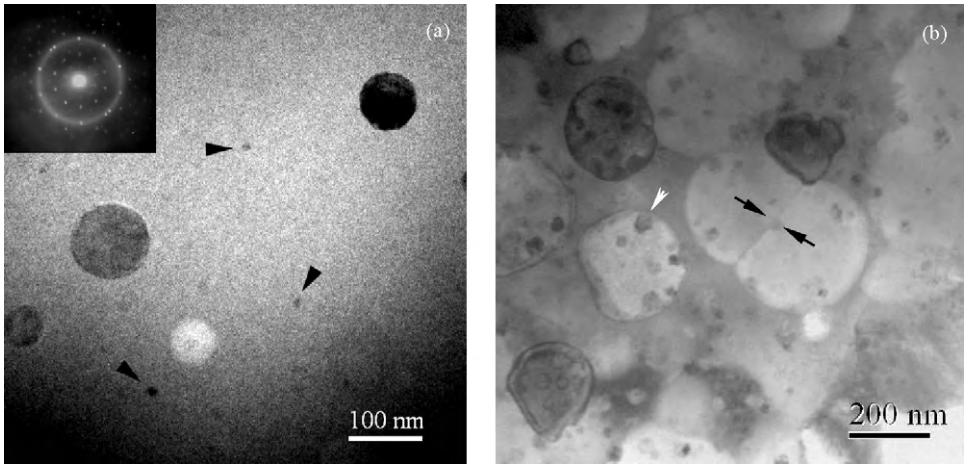

Fig. 3. (a) Bright field TEM image showing the microstructure of 703 K-5 min annealed ribbon glass. Spherical I-phase particles were embedded in the glassy matrix (with five-fold SAED pattern as inserted). The black arrowheads point to some very fine nano-particles. (b) Bright field TEM image of the 723 K-5 min annealed microstructure. The two black arrows denote two impinged I-phase grains. The white arrowhead points to a grown nano-particle of the minority nano-phase.

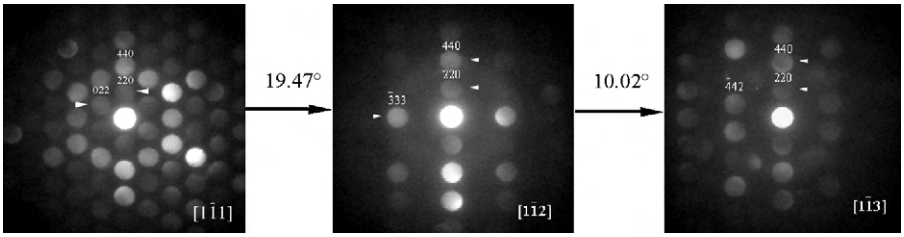

Fig. 4. A series of μ-diffraction patterns of the η-Zr_2Ni type phase formed in the 723 K-5 min annealed ribbon glass.

annealed sample reproduces the 723 K-30 min diffraction profile fairly well. TEM observations were done for clarification of these annealed microstructures.

The bright field TEM image (Fig. 3(a)) shows that spherical particles precipitate in the 703 K-5 min annealed ribbon sample. The inserted five-fold axis electron diffraction pattern of the particles indicates their I-phase nature, which is consistent with the XRD result. The average composition of the I-phase was measured to be approximately $Zr_{59.3}Al_{9.1}Ni_{10}Cu_{19.6}Nb_{2.0}$ using EDX. In comparison with the nominal composition $Zr_{63.7}Al_{9.8}Ni_{9.8}Cu_{14.7}Nb_{2.0}$, the I-phase was enriched with Cu but depleted in Zr. Apart from I-phase, very fine nano-particles are observed in the annealed microstructure as positioned by the arrows in Fig. 3(a). The minority nano-phase was not clearly shown by XRD due to the small volume fraction. Annealing at elevated temperatures for instance at 723 K for 5 min, the I-phase grains grow up and some of them impinge with each other (Fig. 3(b)). While the minority nano-phase was still not detectable by XRD (Fig. 2(a)), the bright field TEM image shows a large amount of them. Extensive μ-diffraction demonstrated that the nano-phase has a η-Zr_2Ni type structure (Fig. 4). The lattice constant was calculated to be $a = 1.226$ nm using the XRD peak positions (Fig. 2(a)). A thorough μ-diffraction investigation on the minority nano-particles has also exposed the existence of a very small amount of tI–Zr_2Ni phase. Kündig et al. found that in the early stage crystallization of a $Zr_{52.5}Cu_{17.9}Ni_{14.6}Al_{10}Ti_5$ metallic glass, a small amount of tI–Zr_2Ni was precipitated together with the majority η-Zr_2Ni phase [16]. With the 3D atomic probe composition analysis evidence, they suggested that a certain oxygen impurity level of the sample would account for the co-precipitation of the two nano-phases.

The BMG samples of this alloy were isothermally annealed at 673 K and 723 K. The XRD patterns of the annealed microstructures are shown in Fig. 2(b). At 673 K, I-phase formation was observed in the 30 min annealed sample. The microstructure of the 723 K-6 min annealed sample is shown in Fig. 5. I-phase grains of about 1 μm in size grew out, showing regular facets. The flower-like diffraction contrast image (circled) in Fig. 5(a) corresponds to the diffraction condition given by the inserted SAED pattern. When tilting the flower-like crystal into another crystallographic orientation, the morphology of the flower changes (Fig. 5(b)). In the double tilting process, the precise location of the flower was referred to a zigzag crack. The diffraction contrast change thus indicates that the flower is a mixture of two different but coherently coexisted phases. Their serial SAED patterns were obtained using double tilting (Fig. 6). By means of reciprocal space reconstruction, they were demonstrated to be the Al_2Zr_3 phase and an unknown primitive cubic (cP) phase ($a = 0.76$ nm). The cP phase has never been reported elsewhere in the literature. The first stage crystallization products of BMG are therefore demonstrated to be different from those of the ribbon glass. In each case, however, the I-phase precipitates as the majority phase.

The I-phase grains are in nanometer size when the phase forms in the first stage crystallizations of the ribbon glass and the BMG samples. Following Frank's hypothesis, the undercooled liquid/I-phase interfacial energy would be small, resulting in a very small I-phase nucleation barrier. This would consequently lead to a high nucleation rate of I-phase and account for the nanometer scale microstructure. The I-phase grains are spherical when they grow out from the ribbon glass. During prolonged annealing, these grains grow up and impinge with each other due to the high particle density. The I-phase grains appear as regular facet in the 723 K-6 min annealed BMG sample. It has been demonstrated that the icosahedral order in an I-phase forming liquid gets well developed with continued and increased undercooling [17–19]. BMGs are made at slow cooling conditions. It is therefore at a slow cooling rate the undercooled liquid could find more available relaxation time

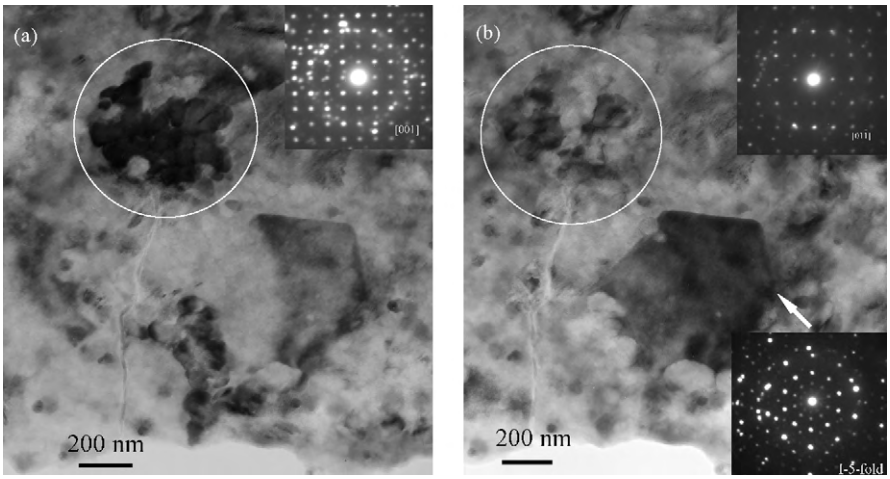

Fig. 5. (a) Bright field TEM image showing the microstructure of 723 K-6 min annealed BMG sample. The SAED pattern of the circled flower is shown in the inset. (b) Bright field TEM image showing the diffraction contrast image produced with the [0 1 $\bar{1}$] zone axis parallel to the incident electron beam. The white arrow points to an I-phase grain with the corresponding SAED pattern as inset in the lower right corner.

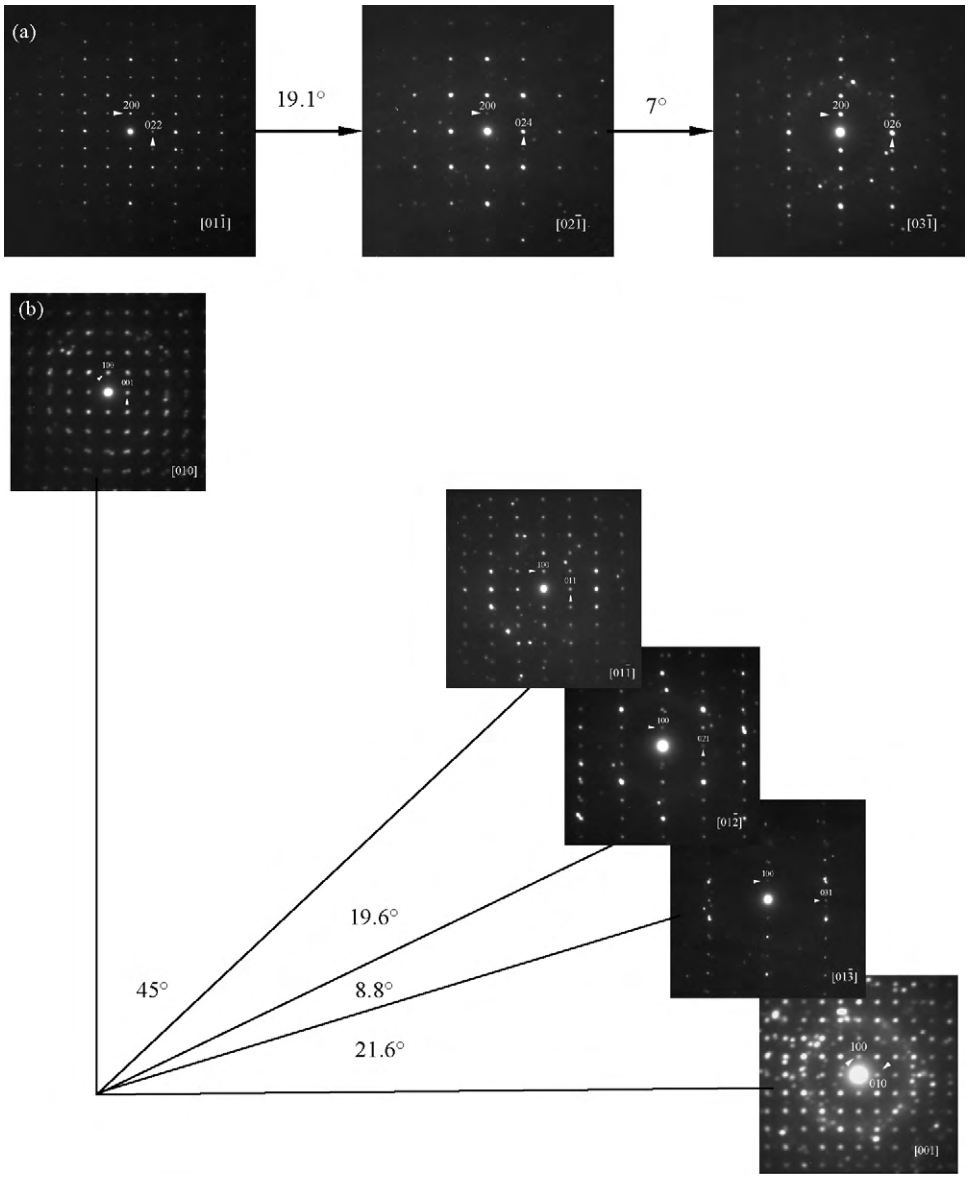

Fig. 6. (a) A series of SAED patterns of the Al_2Zr_3 phase. The angles between different zone axes are experimental values. (b) A stereo arrangement of the SAED patterns of the unknown primitive cubic (cP) phase. The angles between different zone axes are experimental values.

to make an ordered spatial arrangement of the icosahedral atomic clusters, and the formation of well faceted I-phase grains is likely to occur. On the other hand in order to make BMG at this composition, a sufficient fast liquid cooling rate has to be imposed to block the extension of the local icosahedral order in the undercooled liquid.

The crystalline counterparts, namely, the η-Zr_2Ni phase and the Al_2Zr_3 and cP phases, of the ribbon and the BMG samples of the alloy are structurally quite different. The latter two phases cannot be obtained through a displacement phase transformation from the former. Compositionally, the two groups of crystalline counterparts are quite different, though they can grew out from the undercooled liquid of the same composition at the same annealing temperature. In this alloy, composition partitioning is a necessary condition for I-phase formation because the I-phase composition has been revealed to be different from the alloy composition. The stability temperature and the composition range of the I-phase would serve for the understanding the different crystallization behaviors, but these are not fully revealed in our experiments. The existing experimental evidence, however, indicates that the liquid cooling rate for sample preparation has a significant effect on the crystallization behavior of the alloy glass. Another important thermal parameter, the liquid quenching temperature is not taken into considered in the present work. Its effect on the subsequent crystallization behavior of this metallic glass will be studied in the future work.

4. Conclusions

In the first stage crystallization of the $(Zr_{65}Al_{10}Ni_{10}Cu_{15})_{98}Nb_2$ ribbon glass, I-phase and the η-Zr_2Ni-type nano-phase precipitate. For its BMG alloy in this stage, I-phase precipitated with the coherently coexisted Al_2Zr_3 and cP ($a = 0.76$ nm) phases. The formation of metastable I-phase from the undercooled liquid implies that the suppression of the long-range spatial extension of icosahedral order in the undercooled liquid is essential for BMG formation at this composition. The different crystalline phases identified in the ribbon and bulk samples indicate that the cooling rate for metallic glass preparation has a significant effect on its subsequent crystallization behavior.

Acknowledgements

The authors Y.M. Wang, Q. Wang and C. Dong thank the financial support from the National Science Foundation of China (Nos. 50631010 and 50901012) and the National Basic Research Program of China (No. 2007CB613902).

References

[1] A. Inoue, Acta Mater. 48 (2000) 279.
[2] W.L. Johnson, MRS Bull. 24 (1999) 42.
[3] W.H. Wang, C. Dong, C.H. Shek, Mater. Sci. Eng. R44 (2004) 45.
[4] U. Köster, J. Meinhardt, S. Roos, H. Liebertz, Appl. Phys. Lett. 69 (1996) 179.
[5] B.S. Murty, D.H. Ping, K. Hono, A. Inoue, Acta Mater. 48 (2000) 398.
[6] B.S. Murty, D.H. Ping, K. Hono, A. Inoue, Scripta Mater. 43 (2000) 103.
[7] A. Inoue, Mater. Trans. JIM 40 (1999) 1181.
[8] M.W. Chen, T. Zhang, A. Inoue, Appl. Phys. Lett. 75 (1999) 1697.
[9] A. Inoue, T. Zhang, M.W. Chen, T. Sakurai, J. Mater. Res. 15 (2000) 2195.
[10] J. Saida, J. Phys.: Condens. Matter 13 (2001) L73.
[11] L.Q. Xing, T.C. Hufnagel, J. Eckert, W. Löser, L. Schultz, Appl. Phys. Lett. 77 (2000) 1970.
[12] C. Fan, C.F. Li, A. Inoue, Appl. Phys. Lett. 79 (2001) 1024.
[13] F.C. Frank, Proc. R. Soc. Lond. 215A (1952) 43.
[14] L.Q. Xing, J. Eckert, W. Löser, L. Schultz, Appl. Phys. Lett. 73 (1998) 2110.
[15] Z. Altounian, R.J. Shank, J.O. Strom-Olsen, J. Appl. Phys. 61 (1987) 149.
[16] A.A. Kündig, M. Ohnumaa, T. Ohkuboa, K. Hono, Acta Mater. 53 (2005) 2091.
[17] D. Holland-Moritz, D.M. Herlach, K. Urban, Phys. Rev. Lett. 71 (1993) 1196.
[18] K. Urban, D. Holland-Moritz, D.M. Herlach, B. Grushko, Mater. Sci. Eng. A 178 (1994) 293.
[19] K.F. Kelton, G.W. Lee, A.K. Gangopadhyay, R.W. Hyers, T.J. Rathz, J.R. Rogers, M.B. Robinson, D.S. Robinson, Phys. Rev. Lett. 90 (2003) 195504.